ENHANCING THE DIRECTIVITY OF PHASED ARRAY ANTENNAS USING LENS-ARRAYS

Abbas Abbaspour-Tamijani[1, *], Lisha Zhang[2], and Helen K. Pan[3]

[1]Freeform Wave Technologies, LLC, Newport Beach, CA, USA

[2]School of Electrical, Computer, and Energy Engineering, Arizona State University, Tempe, Arizona, USA

[3]Intel Lab, Intel Corporation, Santa Clara, CA, USA

Abstract—Small phased-array antennas can be combined with dielectric lenses or planar lens-arrays to form directive beam-steering system. The use of the lens increases the size of the radiating aperture and enhances the directivity of the phased array, but it also reduces its scan field of view. However, the effect can be controlled by properly designing the phase delay profile across the lens. This paper presents the formulation and methodology for designing modified lenses that can allow the desired scan angle. The utility and limitations of the proposed approach will be illustrated by considering several design examples. Simulations suggest that a directivity enhancement of $> 2\,\mathrm{dB}$ and wide scan field of view (up to $45°$ off boresight) can be obtained for compact radiation systems employing small lenses and short separations between the lens and phased array. Larger directivity improvements in the range of tens of dB's are possible in systems with limited scanning capability by employing large lenses and greater phased array-lens separation. Ease of implementation and the ability of the proposed topology to adapt to the system requirements make this topology an interesting candidate for various millimeter-wave radio applications.

1. INTRODUCTION

Research on integrated circuit phased-array transceivers for millimeter-wave applications has seen major progress in the past few years and an increasing number of groups from both academia and industry have

successfully demonstrated such systems in frequencies ranging from 18 to 77 GHz [1–5]. However, practical limitations such as the die size, RF losses of on-chip transmission lines and power dividers/combiners, and DC power consumption present serious obstacles in scaling these designs for arrays with more than a few dozen elements. These limitations can dramatically reduce the utility of the phased array approach for longer range applications where antenna gain constitutes an important term in the link budget calculations.

Theoretically, the number of phase shifters can be reduced by using subarray techniques [6–8], which can address some of the above mentioned concerns. But subarraying introduces new limitations: (1) It dramatically reduces the scan field of view, (2) due to the required overlapping between the subarrays [8] the transmission line implementation of the feed network is quite complicated in the case of 2D arrays, and (3) the loss of the feed network can quickly offset any improvements in the directivity for larger arrays. Free-space feeding techniques can alleviate the last two problems, but they are not suitable for compact implementations and do not help with the reduced scan field of view.

An alternative approach, which is in some ways related to subarraying but builds on a different principle, is to use the phased array antenna in tandem with a planar lens [9]. Commonly, the beam in lens-based systems is steered by switching the signal between an array of feed elements arranged on the lens focal surface [10, 11]. This configuration generally requires a significant distance between the feed array and the lens, leads to a discrete number of beam positions (equal to the number of feed antennas), and needs RF switches. By contrast, the proposed topology replaces the switchable feed array by a single phased array antenna that generates a steerable spherical wavefront. The lens, that is usually significantly larger than the phased array, transforms this spherical wavefront to a planar one. As the area of the lit region on the lens is greater than the phased array, the result is a net boost in directivity.

Replacing the feed array with the phased array offers several advantages: (1) It eliminates the need for RF switches, (2) it reduces the depth of the system (from F to G, see Fig. 1), (3) it enables continuous scanning, (4) it allows a more efficient use of the aperture in the focal plane array, and (5) it provides a natural means of power combining if each element in the phased array is coupled to a dedicated power amplifier. These characteristics are highly desirable in practice and make the proposed topology a very interesting one for millimeter-wave applications. We refer to the proposed configuration as the Lens-Enhanced Phased-Array (LEPA) configuration.

This paper examines the utility of the LEPA configuration via analysis and by considering a hypothetical example where the lens is implemented as a planar lens-array. A brief description of the proposed embodiment and the analysis approach are presented in Section 2, followed by the preliminary results and discussions for a standard single focus lens-array in Section 3. The methodology for modifying the lens design is presented and the impact of the lens modification is demonstrated by examples in Section 4. Additional examples for some application scenarios are provided in Section 5.

2. TOPOLOGY AND ANALYSIS METHOD

2.1. ALEPA Topology

The geometry of a LEPA beam steering system is shown in Fig. 1, where O, G, and F indicate the lens (lens-array) center or apex, phased-array center, and lens' focal point, respectively, all lying on a line that can be referred to as the main optical axis. The lens and phased-array are parallel to each other and perpendicular to this axis. F denotes the nominal focal distance of the lens and G represents the distance between the lens and phased array ($G < F$). The global coordinate system is attached to the outer surface of the lens, with the
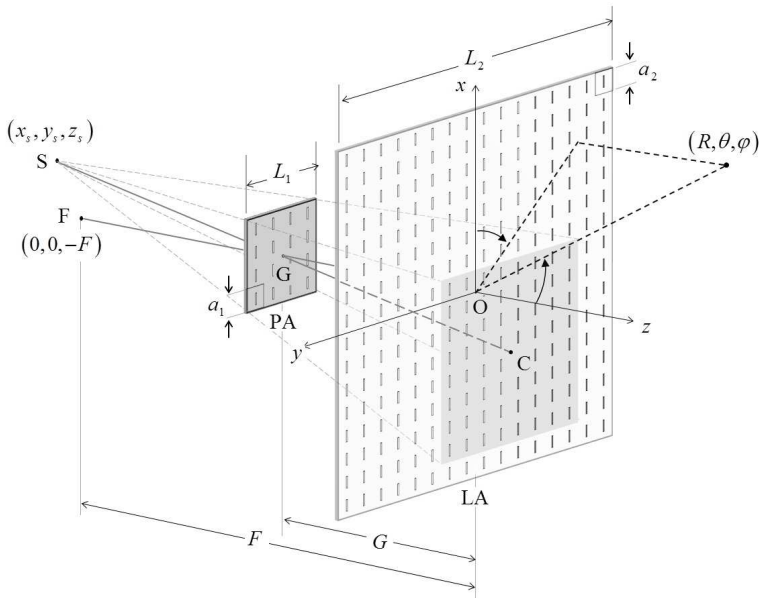
Figure 1. Geometry of a LEPA based on a planar lens-array.

z axis being aligned with the main optical axis.

In general, the lens antenna can be implemented as a dielectric lens, a Fresnel lens, or a lens-array. However, planar implementations are preferable in view of their simplicity and practical benefits. Although Fig. 1 depicts a lens-array based implementation and the analysis approach that will follow has been tailored for a particular lens-array design, the theoretical discussions and findings presented in this paper are general and apply to all embodiments of the system. Moreover, as the lens functions as a focusing device, it is easy to envision variants of the proposed topology based on reflectors or reflectarrays (provided that the system can be effectively implemented for an offset-fed configuration to minimize blockage). Having this in mind, for simplicity, throughout the rest of this paper we will focus our attention on lens-array based LEPA's and use the abbreviations PA and LA (or lens) to refer to the phased array and lens-array, respectively.

For the case of a boresight beam, the phases of the PA elements are chosen as if they were excited by a point source located at F. Under such an excitation the PA output aperture will constitute an approximate Huygens equivalent source for the point source and produces a forward radiating pseudo-spherical wavefront that appears as if emanating from the focal point. The lens then collimates this spherical wavefront into a narrow beam propagating in the z direction. As the PA has a finite area and does not entirely encompass the point source it replaces, the resulting spherical wave is also imperfect (truncated) and illuminates only a portion of the lens effectively. From a purely geometrical standpoint, the "lit region" of the lens (LR) can be found by projecting the phased array boundary on the lens surface with reference to F. As the area of the lit region is greater than that of the phased array by a factor of $\alpha^2 = F^2/(F - G)^2$, directivity is expected to increase by the same factor.

For a scanned output beam, PA elements are phased such that they produce spherical wavefronts emanating from virtual point sources located off the lens axis. As moving the virtual point source changes the location of the lit region in the lens plane, the LA area must be chosen significantly larger than α^2 times that of PA. We will see later that the relationship between the location of the virtual point sources and output beam angle is an important design parameter that affects the system performance. Here, we suffice to point out that due to the movements of the lit region, the methods of locating the feed point vs. scan angle that are customary in simple lens or reflector systems cannot be used to determine the required location of the virtual point source in the case of LEPA.

2.2. Analysis Method

To enable a quantitative evaluation of the proposed topology, we consider a LEPA configuration where the PA is implemented as an array of x-directed electric dipoles and the LA is implemented as an array of slot-based antenna-filter-antenna (AFA) elements [12, 13], with y-directed slot antennas on the side facing PA and x-directed slot antennas on the opposite side.

Lens-array structures are often electrically very large and cannot be analyzed using full-wave simulations in one piece. Although they are finite and made of dissimilar AFA cells, the design procedure usually relies on periodic array simulations to characterize the reflection and transmission coefficients of the AFA elements. For analysis, Friis' formula and geometric distance between AFA elements and the feed antenna are used to calculate the complex amplitude of the incident wave at the input of each AFA cell and the simulated element transmission coefficients are utilized to reconstruct the aperture distribution over the output side of the LA and, in turn, the far field. For simple feed and LA systems, it has been shown that this hybrid analysis method produces accurate predictions of the overall gain and radiation pattern for observation angles within the main lobe and first two sidelobes [13]. In the case of LEPA, where the distance between LA and PA can be much smaller, the method can be modified by using a Green's function calculation instead of Friis' formula to find the input amplitude for each AFA element. This modified formalism is presented below.

To reproduce a spherical wavefront emanating from a virtual source S, the input current of the m'th x-directed dipole in the PA is chosen as:

$$I_m^d = I_0 e^{-j\varphi_m}; \quad \varphi_m = k\sqrt{(x_m' - x_s)^2 + (y_m' - y_s)^2 + (G + z_s)^2} \quad (1)$$

where $(x_m', y_m', -G)$ and (x_s, y_s, z_s) represent the coordinates of the dipole and the virtual source, respectively. Clearly, (1) assumes that the magnitude of the input current is the same for all PA elements.

The received signals in each of the slot antennas facing the PA can be represented by its induced short circuit current, defined as the current flowing between its terminals as result of the incident field under short circuit conditions. If l^d and l^s denote the physical lengths of the dipoles and slots, respectively, the short circuit current induced

in the n'th y-directed slot centered at $(x_n, y_n, 0)$ is given by:

$$I_n^{sc} = \sum_{m=1}^{M} I_m^d \left[\int_{-\frac{l^d}{2}}^{\frac{l^d}{2}} dx \int_{-\frac{l^s}{2}}^{\frac{l^s}{2}} dy \bar{I}^d(x) \bar{V}^s(y) g_{mn} e^{jk \sin \theta_{mn}(x \cos \varphi_{mn} - y \sin \varphi_{mn})} \right] \quad (2)$$

where the summation is over the PA elements, and:

$$\bar{I}^d(x) = \sin k \left(\tfrac{1}{2} l^d - |x| \right) / \sin k \left(\tfrac{1}{2} l^d \right)$$
$$\bar{V}^s(y) = \sin k \left(\tfrac{1}{2} l^s - |y| \right) / \sin k \left(\tfrac{1}{2} l^s \right)$$
$$g_{mn} = \frac{-jke^{-jkR_{mn}}}{4\pi R_{mn}} \left[1 + (jkR_{mn})^{-1} \right] \cos \theta_{mn}$$
$$R_{mn} = \sqrt{(x_n - x_m')^2 + (y_n - y_m')^2 + G^2}$$
$$\theta_{mn} = \cos^{-1} (G/R_{mn})$$
$$\varphi_{mn} = \cos^{-1} \left[(x_n - x_m') \Big/ \sqrt{(x_n - x_m')^2 + (y_n - y_m')^2} \right] \operatorname{sgn}(y_n - y_m')$$

where k is the free-space wave number. Equation (2) assumes that the slots lie in the Franhofer zone of the dipole elements, but it does not require $kR_{mn} \gg 1$. It also neglects the mutual coupling effects between the PA elements or between the LA elements. For short dipole and slot lengths, (2) can be simplified to:

$$I_n^{sc} \approx \sum_{m=1}^{M} \frac{l^d l^s}{4} g_{mn} I_m^d \quad (3)$$

Neglecting the insertion loss of the AFA elements, the output voltage at the center of the x-directed slot n is given by:

$$V_n^{s'} = V_n^s e^{-j\Delta_n} = \frac{1}{2} Z^s I_n^{sc} e^{-j\Delta_n} \quad (4)$$

where Z^s is the impedance of the slot antennas and Δ_n the phase delay of the n'th AFA. Equations (3) and (4) can be combined and written in the matrix form, as:

$$\left[V_n^{s'} \right] = [A_{nm}] \left[I_m^d \right]; \quad A_{nm} = \frac{Z^s l^d l^s}{8} g_{mn} e^{-j\Delta_n} \quad (5)$$

which relates the LA output coefficients to the PA excitation currents.

In view of reciprocity, the open circuit voltages established across the dipoles in the receive mode are given by:

$$[V_m^{oc}] = [A_{nm}]^T \left[I_n^{sc'} \right] \quad (6)$$

where $I_n^{sc'}$ denotes the short circuit current induced in the n'th x-directed slot (on the outer face of LA) as a result of the impinging wave.

The voltages $[V_n^{s'}]$ can be used to find the radiated far field and output array factor. At a far field point (R, θ, φ), the magnetic field H can be written as:

$$\vec{H}^{FF} = -j\omega\varepsilon_0 \frac{l^s e^{-jkR}}{8\pi R} \left(\cos\theta\cos\varphi\hat{\theta} - \sin\varphi\hat{\varphi} \right) AF(\theta, \varphi);$$

$$AF(\theta, \varphi) = \sum_{n=1}^{N} V_n^{s'} e^{jk\sin\theta(x_n\cos\varphi + y_n\sin\varphi)}$$

(7)

Here, AF represents the array factor, and it may be calculated directly in terms of the spectral variables $\xi = \sin\theta\cos\varphi$ and $\eta = \sin\theta\sin\varphi$ using a two-dimensional Fast Fourier Transform (FFT) algorithm. The total radiated power and maximum directivity can be calculated as:

$$P_{rad} = \int_0^{2\pi} d\varphi \int_0^{\pi/2} \frac{\eta}{2} \left| R\vec{H}^{FF} \right|^2 \sin\theta d\theta$$

$$= \frac{k^2 l_s^2}{32\eta} \iint_{\xi^2 + \eta^2 \leq 1} |AF(\xi, \eta)|^2 \frac{1 - \xi^2}{\sqrt{1 - \xi^2 - \eta^2}} d\xi d\eta$$

(8)

$$D_{\max} = \frac{4\pi \max\left[|AF(\xi, \eta)|^2 \left(1 - \xi^2 \right) \right]}{\iint_{\xi^2 + \eta^2 \leq 1} |AF(\xi, \eta)|^2 \frac{1 - \xi^2}{\sqrt{1 - \xi^2 - \eta^2}} d\xi d\eta}$$

(9)

It must be noted that neglecting mutual coupling in the above analysis has little impact on the accuracy of the calculated directivity and radiation pattern, which are of primary interest for the purpose of this paper. In the PA, the presence of mutual coupling between elements only affects the actual element excitations that must be applied to produce the amplitudes given by (1), not the PA amplitudes themselves. Also for the LA, in practice, the exponential term in (4) is replaced by the element transmission coefficients that are obtained from periodic structure simulations which, in an approximate sense, include the effects of coupling from adjacent AFA elements. In a good LA design with compact cell dimensions, these coefficients are fairly insensitive to the angle of arrival [12], which means the transmission coefficient is simply a frequency dependent constant and will not affect the output aperture distribution or radiation pattern. The mutual coupling between the PA and LA elements has been effectively taken into account by the use of Green's functions.

3. RESULTS FOR LEPA WITH STANDARD LENS

To start, we examine the performance of a hypothetical LEPA system based on a standard LA. The term "standard LA", for the purpose of this paper, refers to a single focus lens-array that is designed to produce perfect uni-phase output coefficients when excited by an ideal point source at its focal point $(0, 0, -F)$. Such a lens is described by a phase delay function in the form of:

$$\Delta_n = -k\sqrt{x_n^2 + y_n^2 + F^2} + \Delta_0 \tag{10}$$

where $(x_n, y_n, 0)$ and Δ_n specify the center coordinates and phase delay of the AFA element n and Δ_0 is an arbitrary constant.

If the LEPA system works as expected, the enhancement resulting from the use of lens will be given by the squared of α:

$$\alpha = \frac{F}{F - G} \tag{11}$$

that represents the linear magnification factor from PA to the lit region of LA. Hence, for a given PA-LA distance G, F can be found from the desired value of α as:

$$F = \frac{G}{1 - 1/\alpha} \tag{12}$$

This principle has been used to design a LEPA system with a 16-element (4×4) PA and 576-element (24×24) LA for a directivity enhancement factor of 2 ($\alpha = 1.41$). The PA and LA specifications are summarized in Table 1, where λ is the free space wavelength. The values of the PA phase $\{\angle I_m^d\}$ calculated for a virtual source located at the focal point F as well as the simulated LA output amplitudes $\{|V_n^{s'}|\}$ and phases $\{\angle V_n^{s'}\}$ and radiation pattern are shown in Fig. 2. As expected, the output beam in this case points to the boresight direction, and directivity is 20.3 dBi, which is 3.4 dB higher than the value found for the PA alone (16.9 dBi). The boundary of the geometrically found lit region is marked on the aperture distribution plots.

Table 1. Example LEPA parameters.

Phased Array			Lens-Array		
No. of elements	M	16	No. of elements	N	576
Array side length	L_1	2λ	Array side length	L_2	12λ
Array spacing	a_1	0.5λ	Array spacing	a_2	0.5λ
PA-LA distance	G	2λ	Focal length	F	6.8λ
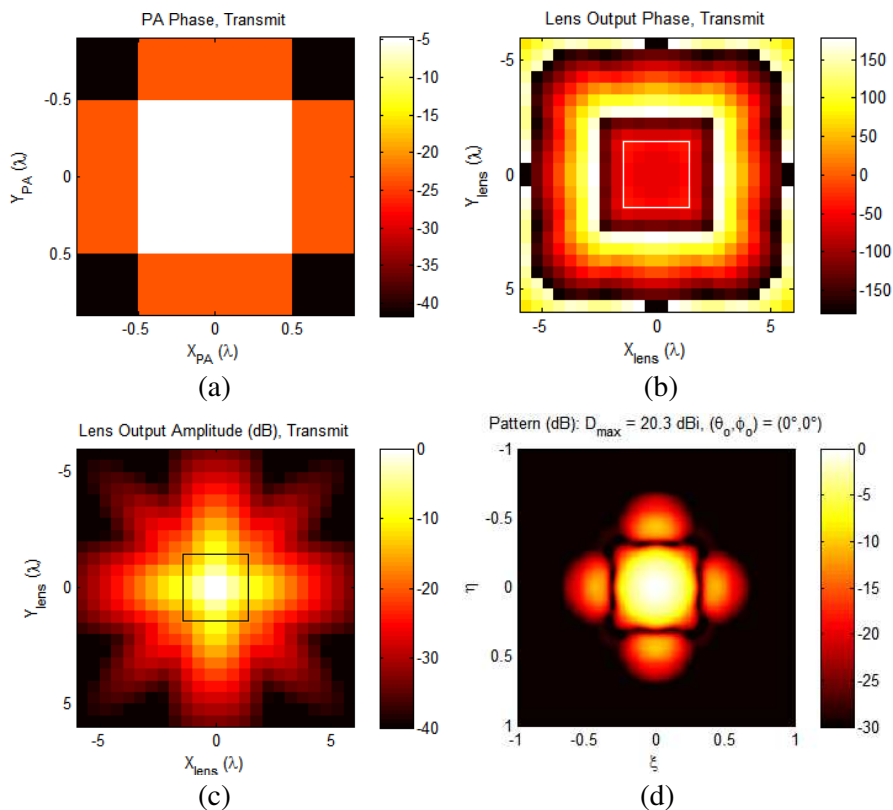
Figure 2. Simulation results for LEPA with standard LA, set for boresight radiation: (a) PA phase profile, (b) LA output phase, (c) LA output amplitude, and (d) radiation pattern. The "lit region" is marked by the squares in (b) and (c).

In the case of a simple LA with a low-gain (point-source-like) feed, to scan the beam to (θ_s, φ_s) the feed must be positioned at $(-F \tan \theta_s \cos \varphi_s, \ -F \tan \theta_s \sin \varphi_s, \ -F)$. However, the same choice of placement for the virtual source in the case of the LEPA system does not produce the desired result, as demonstrated in Fig. 3. The intended value of scan in this example was $(45°, 45°)$ and, accordingly, the virtual source point was moved to $(-F/\sqrt{2}, \ -F/\sqrt{2}, \ -F)$. The peak radiation occurs at $(\theta_o, \varphi_o) = (22°, 45°)$. Although the directivity is more than 7 dB higher compared to the simple PA scanned to the same angle (16.5 dBi), the output beam tilt is considerably smaller than the desired value. Further analysis shows that the reduced scan is related to the way LA transforms an incident spherical wavefront to plane wave. This fact will be demonstrated below.

(a)

(b)

(c)

(d)
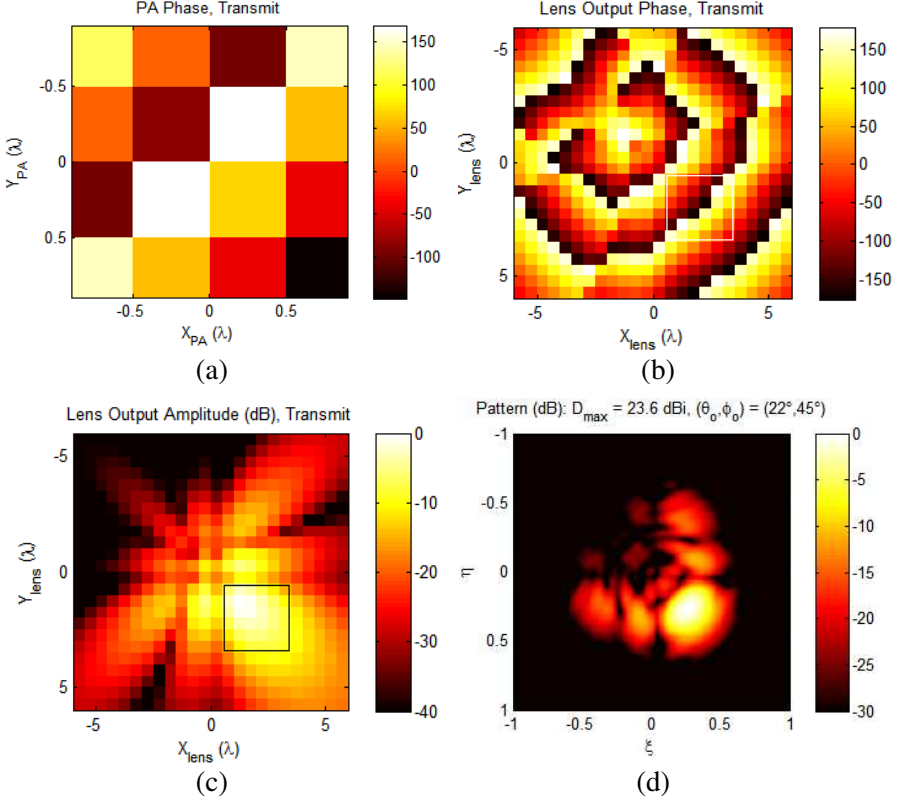
Figure 3. The LEPA system of Fig. 2 resimulated with the virtual source moved to $x_s = y_s = -4.8\lambda$, $z_s = -6.8\lambda$.

For simplicity let us ignore the discrete nature of phase transformation in LA and assume a continuous phase delay profile $\Delta(x, y)$. The relationship between the input and output phase (x, y) can be expressed as:

$$\psi^o(x, y) = \psi(x, y) + \Delta(x, y) \tag{13}$$

where $\psi(\cdot)$ and $\psi^o(\cdot)$ are the negative of the phase distributions over the input and output lens surfaces, respectively. If (x_c, y_c) denotes the center of the lit region, the direction of the output wave can be found by equating the derivatives of $\psi^o(\cdot)$ with respect to x and y to the corresponding component wave numbers:

$$\begin{aligned}
\psi_x(x_c, y_c) + \Delta_x(x_c, y_c) &= k\xi_o \\
\psi_y(x_c, y_c) + \Delta_y(x_c, y_c) &= k\eta_o
\end{aligned} \tag{14}$$

where the subscripts x and y indicate derivatives with respect to these variables. For a virtual source located at $(x_s, y_s, z_s) = (-F \tan \theta_s \cos \varphi_s, -F \tan \theta_s \sin \varphi_s, -F)$, we have:

$$\psi(x, y) = k\sqrt{(x - x_s)^2 + (y - y_s)^2 + F^2} \tag{15}$$

and the coordinates of center of the lit region may be found as $x_c = -\beta x_s$ and $y_c = -\beta y_s$, where $\beta = \alpha - 1$. Assuming a standard lens with $\Delta(x, y)$ in the form of:

$$\Delta(x, y) = -k\sqrt{x^2 + y^2 + F^2} + kF \tag{16}$$

(14) yields:

$$\begin{aligned}
\xi_o &= \left(1 - \beta \Big/ \sqrt{\beta^2 + \alpha^2 \cos^2 \theta}\right) \sin \theta_s \cos \varphi_s \\
\eta_o &= \left(1 - \beta \Big/ \sqrt{\beta^2 + \alpha^2 \cos^2 \theta}\right) \sin \theta_s \sin \varphi_s
\end{aligned} \tag{17}$$

or:

$$\varphi_o = \varphi_s$$
$$\theta_o = \sin^{-1}\left[\left(1 - \beta \Big/ \sqrt{\beta^2 + \alpha^2 \cos^2 \theta_s}\right) \sin \theta_s\right] \tag{18}$$

Equation (18) clearly predicts that θ_o is always smaller than θ_s (since the expression inside parenthesis is smaller than unity). This means that the excitation wavefront generated by the virtual source is refracted towards the main optical axis as it passes through the lens. Although the above derivation is only for the case of standard lens with virtual source scanning in the focal plane, the stated conclusion is true for any convex lens. This phenomenon restricts the attainable scan field of view and is a fundamental limitation of LEPA systems.

As predicted by (18), the compression in the scan field of view is not linear and becomes more severe as θ_o approaches its maximum value. A welcome result of this situation is an improvement in directivity for the scanned beam positions. This effect can counter balance the scan loss mechanisms that generally worsen with the increase in the scan angle.

For the example of Fig. 3, (18) predicts a peak at $\theta_o = 26°$. The discrepancy with the simulation is due to the approximate nature of the above formulation, which relies on simple geometrical relationships to determine the center of the lit region and assumes that the standard lens can produce a planar wavefront from the spherical incident wave, even if the lit region is not centered at its apex. In reality, variations of the incident field with distance tend to move the lit region closer to O, and the latter assumption is not valid for the standard lens as can be seen by examining the second derivatives of (13) for ψ and Δ given by (15) and (16) at a generic point C with $x_c, y_c \neq 0$. We refer to the

shift and deformation of the lit region as *smudging*. Smudging and the error associated with it reduce if G is much larger than both L_1 and the wavelength.

4. LEPA WITH MODIFIED LENS DESIGN

4.1. Modifying The Lens Design

The inadequacy of the standard lens design in converting off-center spherical wavefronts to planar can be remedied by modifying the lens phase delay profile $\Delta(x, y)$. Since the lens design for a general 2D steerable LEPA must be radially symmetric Δ will be a function of $\rho = \sqrt{(x^2 + y^2)}$ and, without loss of generality, the problem can be formulated for the case of scan in xz plane, implying: $y_s = y_c = \varphi_o = 0$ and $\rho_c = |x_c|$.

The geometrical parameters involved in our formulation are defined in Fig. 4. x_s, z_s, and x_c are all functions of the output scan angle θ_o, but their exact dependence on θ_o is unknown for the moment. Equations for ψ and Δ can be written as:

$$\psi(x, y) = k\sqrt{(x - x_s)^2 + y^2 + z_s^2} \tag{19}$$

$$\Delta(x, y) = \Delta\left(\sqrt{x^2 + y^2}\right) \tag{20}$$

For the lens to produce a wavefront traveling in the direction $\theta = \theta_o$ and $\varphi = 0$, (14) must hold with $\xi_o = \sin\theta_o$ and $\eta_o = 0$. For the above
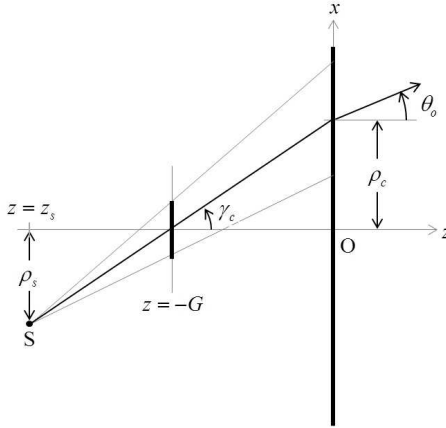
Figure 4. Geometrical setup for modified lens design formulation.

ψ and Δ functions this reduces to a single condition:

$$k\frac{\rho_c/G}{\left[1+\rho_c^2/G^2\right]^{1/2}} + \Delta_\rho\left(\rho_c\right) = k\sin\gamma_c + \Delta_\rho\left(\rho_c\right) = k\sin\theta_o \qquad (21)$$

where we have used the geometrical relationships of Fig. 4 to simplify the equation.

To ensure that the output wavefront approximates a plane wave, the second derivatives of ψ^o with respect to x and y must be set to zero at the center of the lit region:

$$\psi_{xx}\left(x_c,0\right) + \Delta_{xx}\left(x_c,0\right) = -\frac{k}{z_s\left[1+\rho_c^2/G^2\right]^{3/2}} + \Delta_{\rho\rho}\left(\rho_c\right) = 0$$

$$\psi_{yy}\left(x_c,0\right) + \Delta_{yy}\left(x_c,0\right) = -\frac{k}{z_s\left[1+\rho_c^2/G^2\right]^{1/2}} + \frac{\Delta_\rho\left(\rho_c\right)}{\rho_c} = 0 \qquad (22)$$

Equation (22) is independent of the output beam angle and, hence, must hold for any value of ρ_c. They can be treated as differential equations describing $z_s(\rho_c)$ and $\Delta(\rho_c)$, where we have chosen to express the dependence of z_s on θ_o by making it a function of ρ_c which itself depends on θ_o. Solving these equations subject to the condition $z_s(0) = -F$ and $\Delta(0) = 0$ leads to:

$$z_s = -F \qquad (23)$$

$$\Delta\left(\rho\right) = -k\frac{G^2}{F}\left[1+\rho^2/G^2\right]^{1/2} + k\frac{G^2}{F} \qquad (24)$$

(23) states that the virtual source must remain confined to the planar surface $z = -F$ for all scan angles. This is not a trivial conclusion, as in general the focal surface does not need to be planar. (24) gives the phase delay profile for the modified lens design.

The exact location of the virtual source for the desired scan angle θ_o can be found from (21), which after plugging in the expression for $\Delta_\rho\left(\rho_c\right)$ reduces to:

$$\sin\gamma_c = \alpha\sin\theta_o \qquad (25)$$

where γ_c is the incidence angle on the input side of the lens as defined in Fig. 4, and α is given by (11). Hence we find:

$$\rho_s = (F-G)\tan\gamma_c = F\frac{\sin\theta_o}{\sqrt{1-\alpha^2\sin^2\theta_o}} \qquad (26)$$

In the general case of $\varphi_o \neq 0$, clearly, the lens delay Equation (24) remains unchanged and the transversal coordinates of the virtual

source can be expressed as:

$$x_s = -F \sin \theta_o \cos \varphi_o \Big/ \sqrt{1 - \alpha^2 \sin^2 \theta_o}$$
$$y_s = -F \sin \theta_o \sin \varphi_o \Big/ \sqrt{1 - \alpha^2 \sin^2 \theta_o} \tag{27}$$

An upper bound on the scan field of view can be established from (26) by allowing $\gamma_c \to \pi/2$, which leads to:

$$\theta_o < \sin^{-1}(1/\alpha) \tag{28}$$

A tighter bound can be found by confining the lit region to lens area, or:

$$\rho_{c,\text{max}} = (L_2 - \alpha L_1)/2 \tag{29}$$

that gives:

$$\theta_{o,\text{max}} = \sin^{-1}\left[\frac{1/\alpha}{\sqrt{1 + 4G^2 \Big/ (L_2 - \alpha L_1)^2}} \right] \tag{30}$$

4.2. LEPA Example with Modified LA

The above formalism was used to design a lens-array with the parameters of Table 1. The delay profile $\Delta(\rho)$ for this lens is shown in Fig. 5 along with that of the standard lens of the previous section. The simulated results for the boresight and scanned cases are shown in Figs. 6 and 7, respectively. Boresight directivity in this case is 19.5 dBi which is 0.8 dB less than LEPA with standard lens. This reduction is due to the fact that the focusing function of the modified lens is only
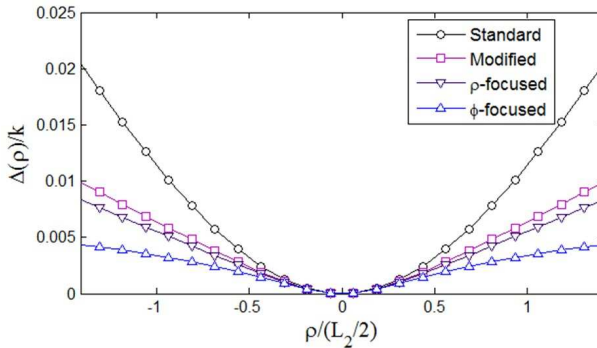

Figure 5. Phase delay profile for various lens designs.
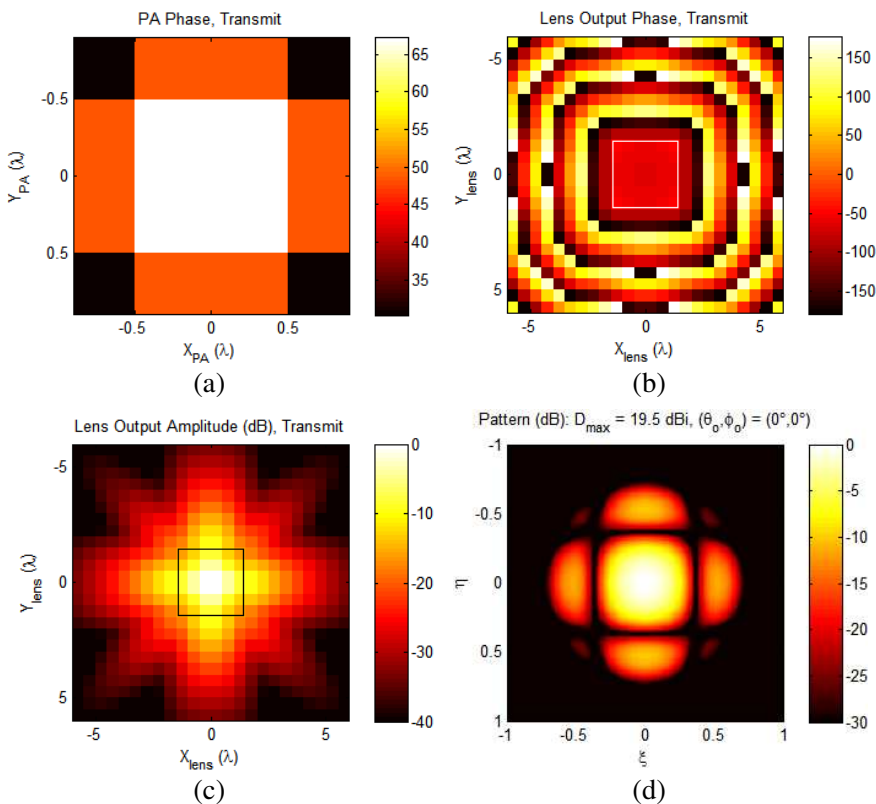
Figure 6. Simulation results for LEPA with modified lens set for boresight radiation: (a) PA phase profile, (b) LA output phase, (c) LA output amplitude, and (d) radiation pattern. The "lit region" is marked by square in (b) and (c).

accurate to the second order, while standard lens has a nearly perfect focusing function when illuminated from its nominal focal point.

The position of the virtual source for the scanned case is chosen as $x_s = y_s = -8\lambda$, $z_s = -6.8\lambda$. These values correspond to scanned theoretical maximum scan angle of $\theta_o = 40.4°$ predicted by (30). The simulated pattern shows a peak directivity of 22 dBi at $(\theta_o, \varphi_o) = (36°, 45°)$. In spite of the reduction in directivity, the scan field of view shows significant improvement compared the LEPA with standard LA. The remaining z-ward skewing of the beam is the result of smudging, which as was mentioned earlier, is also responsible for higher directivity in the scanned case.
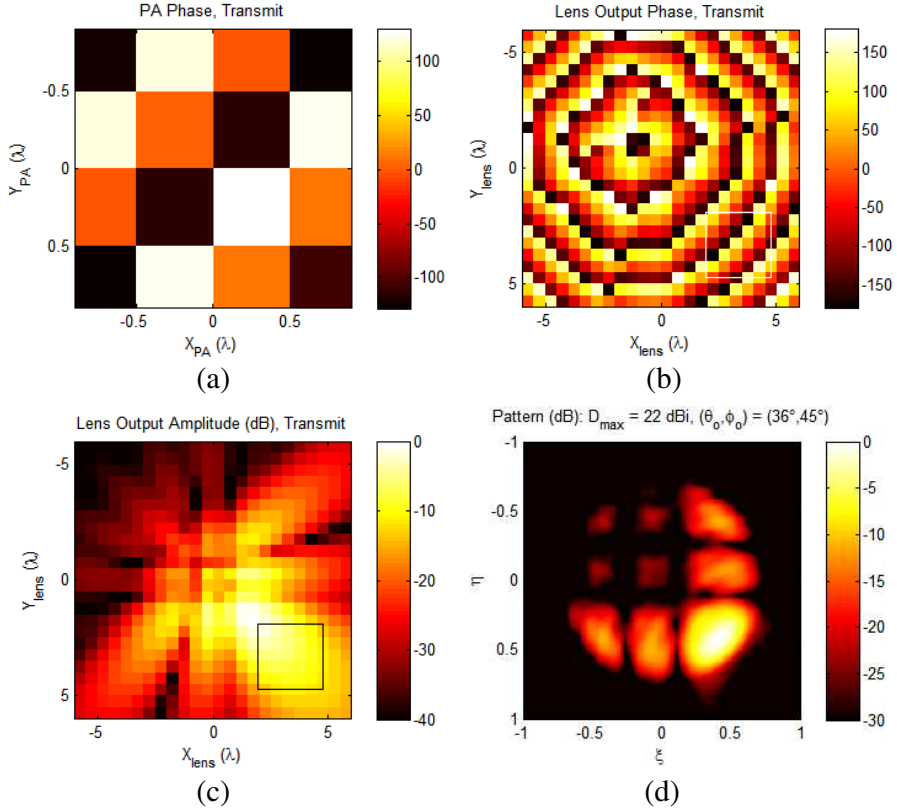
Figure 7. The LEPA system of Fig. 6 resimulated with the virtual source moved to $x_s = y_s = -8\lambda$, $z_s = -6.8\lambda$.

4.3. Single-axis Focusing Lens Designs

The larger directivity boost at oblique beam angles in the previous examples suggests the possibility that the geometrical magnification factor and focusing properties of the lens for off-boresight beam positions can be traded off for a greater scan field of view. Lowering the magnification factor for larger values of scan can be achieved by allowing an ascending $|z_s(\rho_c)|$ function. However, as such a behavior is inconsistent with (23), it is clear that it will at least partly impair the ability of the lens to transform the incident spherical wavefront to a planar wavefront. That is, at best, only one of the Equation (22) can be satisfied. Solving the upper one of (22), corresponds a perfect phase transformation along $\hat{\rho}$ only and leads to the following equation

for $\Delta(\rho)$:

$$\Delta_1(\rho) = \int\limits_0^\rho \int\limits_0^r \frac{k}{z_s(r)\left[1 + r^2/G^2\right]^{3/2}} dr^2 \tag{31}$$

Solving the lower one of (22) corresponds to a perfect phase transformation along $\hat{\varphi}$ only and gives:

$$\Delta_2(\rho) = \int\limits_0^\rho \frac{kr}{z_s(r)\left[1 + r^2/G^2\right]^{1/2}} dr \tag{32}$$

These designs can be recognized as single-axis focusing lenses. In either case, after Δ is known, its first derivative can be used in (21) to find γ_c and from that x_s and y_s.

To find the scan field of view, one must first solve (29), for $\rho_{c,\max}$ by replacing for α from $\alpha = z_s(\rho_{c,\max})/[z_s(\rho_{c,\max}) + G]$, and then use this value of ρ_c in (21) to find the maximum beam angle $\theta_{o,\max}$.

The choice of $z_s(\cdot)$ is somewhat arbitrary, but $|z_s|$ must increase monolithically with ρ_0 to produce the desired effect. A convenient choice that leads to analytical expressions for Δ is:

$$z_s(\rho_c) = -F\left[1 + \rho_c^2/G^2\right]^{1/2} \tag{33}$$

This choice gives:

$$\Delta_1(\rho) = -k\frac{G\rho}{2F}\tan^{-1}\left(\frac{\rho}{G}\right) \tag{34}$$

for the $\hat{\rho}$-focused case, and:

$$\Delta_2(\rho) = -k\frac{G^2}{2F}\ln\left(1 + \rho^2/G^2\right) \tag{35}$$

for the $\hat{\varphi}$-focused case.

For the purpose of demonstration, let us reexamine the example LEPA of Table 1 for the two single axis LA designs with the phase delays profiles of (34) and (35). These delay profiles are plotted in Fig. 5 for the chosen values of F and G and are clearly less convex than both standard and modified lens designs. The theoretical value of $\theta_{o,\max}$ is found as 44.6° for the ρ-focused design and 56° for the φ-focused design.

The output aperture phase distributions and radiation patterns of the LEPA using the φ-focused LA are shown in Fig. 8 for the cases of boresight and scanned beam positions.

The scanned case was simulated for $x_s = y_s = -28.7\lambda$ and $z_s = -18.3\lambda$, corresponding to $\theta_o = \theta_{o,\max} = 55.7°$ and $\varphi_o = 45°$.
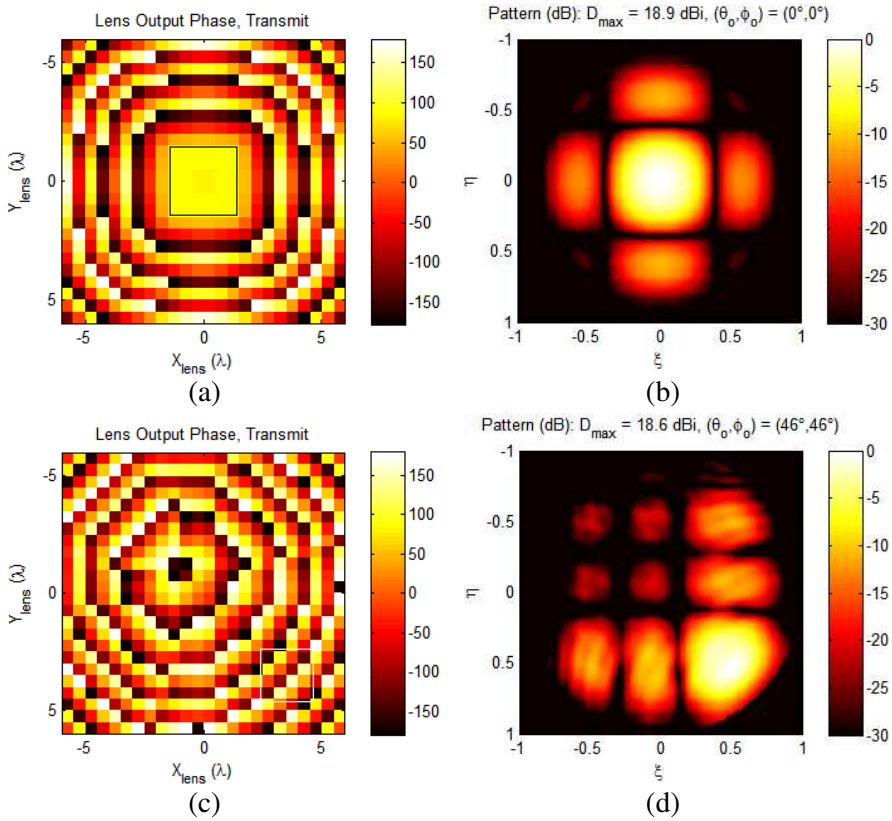
Figure 8. Simulation results for the LEPA with φ-focused LA: (a) LA output phase and (b) radiation pattern for boresight, (c) LA output phase and (d) radiation pattern for $x_s = y_s = -28.7\lambda$, $z_s = -18.3\lambda$.

It can be seen that the area of the lit region on the lens reduces as the beam steers off boresight, which is consistent with the increase in $|z_s|$. The actual peak radiation occurs at $(46°, 46°)$. While the smaller value of θ_o can be explained by smudging, the y-ward skew in φ_o is the direct result of element factor which becomes more noticeable as the beam scans farther away from boresight.

The simulated values of boresight and scanned directivities are 18.9 dBi and 18.6 dBi, respectively, marking enhancements of 2.0 and 3.6 dB compared to a simple 16-element PA scanned to same angles. The lesser boresight directivity compared to the LEPA example with the modified LA (Figs. 6 and 7) is due to the fact that the single-axis focusing device is less effective in collimating the input wavefront.

The boresight directivity can be restored to 19.5 dBi by reducing F to 5λ, which also decreases the actual maximum value of θ_o to $43°$ and the scanned directivity of 18.8 dBi (simulations not shown). For both values of G, the overall directivity experiences a smaller scan loss compared to the simple PA.

5. ADDITIONAL EXAMPLES

Although an experimental demonstration of the LEPA concept is beyond the scope of this article, to illustrate the design procedure and examine the utility of this configuration in various applications we consider three examples.

The first example is a 60 GHz LEPA system for potential applications in notebook and tablet computers. In such applications, the LEPA system has to be implemented with a very small overall depth. A reasonable thickness is $G = 5$ mm. Assuming a 4×4 PA with the spacing $a_1 = 0.45\lambda$ and a 24×24 LA with the spacing $a_2 = 0.5\lambda$, we will have $L_1 = 9$ mm and $L_2 = 6$ cm, and the value of α can be found by solving (30) for these values of L_1, L_2 and G by assuming the desired value of $\theta_{o,\max}$. The PA element spacing has been chosen as 0.45λ to avoid grating lobes in the maximum scan states, considering the fact that the PA scan can be considerably larger than the output beam angle. Also, to account for the smudging effects the $\theta_{o,\max}$ is chosen $\sim 10\%$ larger than the actual desired maximum scan angle. Solving (30) for $\theta_{o,\max} = 50°$ results in $\alpha = 1.28$ and $F = 23$ mm.

Simulated radiation pattern of a LEPA system with the above parameters has been shown in Fig. 9 for four beam positions. The peak directivity is 17.9 dBi in the boresight case and 21.3 dBi for the $(45°, 45°)$ beam. The directivity of the PA alone is estimated at 16.1 dBi at boresight. From these results it is evident that thin LEPA systems with wide angle scan can yield only small values of α and hence their impact on the directivity and overall gain is relatively small. In practice, such a small gain can be easily offset by the insertion loss of the LA or spillover losses. However, the fact that the enhancement is significant for the scanned beam states, suggests that the LA may still be beneficial in countering the effects of scan loss in the PA and extending its effective scan field of view. The boresight directivity can be improved by 0.2 dB for $\alpha = 1.38$ which corresponds to $\theta_{o,\max} = 45°$ and using the ρ-only single-focused LA of (34) to maintain this scan field of view.

In the second example we consider a wireless display (WiDi) application for a flat screen TV or indoor wireless hub. In this case, both the depth and aperture size of the LEPA system can be larger and the required scan angle is somewhat smaller. Solving (34) for
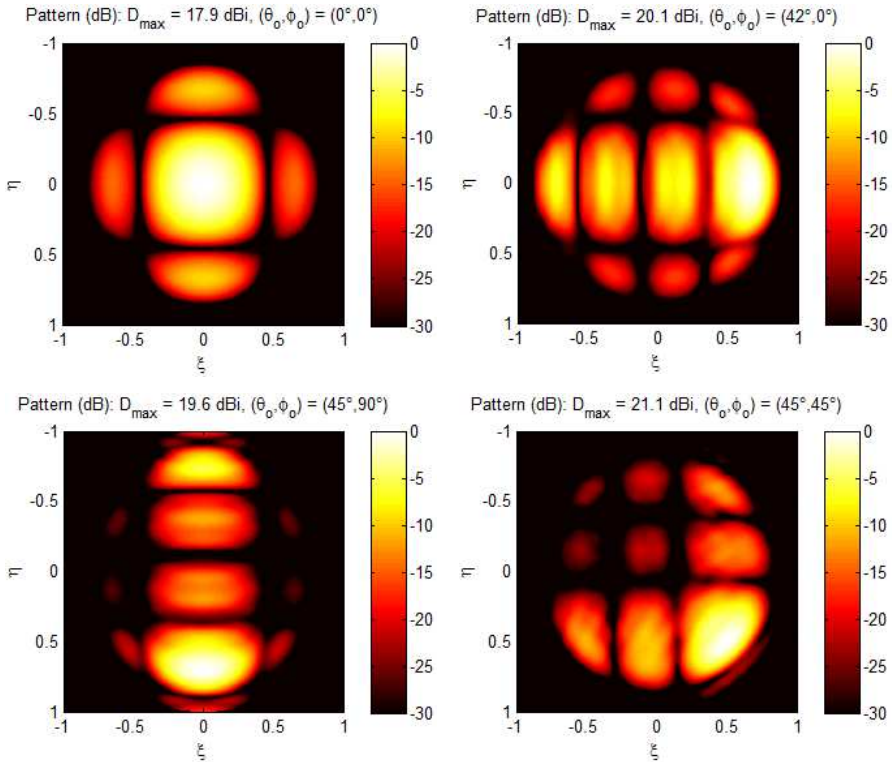
Figure 9. Simulation radiation pattern and peak directivity for a 60 GHz LEPA with $L_1 = 9$ mm, $L_2 = 60$ mm, $G = 5$ mm, and $F = 23$ mm for various scan angles.

$L_1 = 9$ mm, $L_2 = 12$ cm, $G = 2$ cm and $\theta_{o,\max} = 33°$ results in $\alpha = 1.71$ and $F = 4.8$ cm. Simulated radiation patterns for $(0, 0)$ and $(45°, 45°)$ beam angles are shown in Fig. 10. Boresight directivity enhancement in this case is 4.6 dB which is very close to the theoretical value of α^2. The larger L_2 and smaller scan angle in this case allow for an increased directivity enhancement compared to the previous example. A larger value of G, according (30), does not increase α, but it reduces the smudging effect that can impair the desired function of the lens and has a negative effect on directivity.

Finally, we consider a design for the 71–76 GHz E-band wireless backhaul. In backhaul applications, the links are fixed, but electronic steering capability offers an alternative to manual antenna alignment that is necessary for both installation and link maintenance. In this application, the required value of scan field of view is generally small,
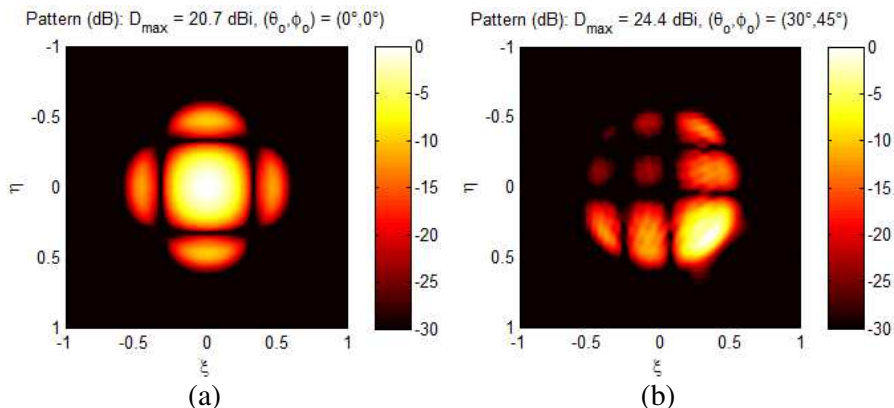
Figure 10. Simulation pattern and peak directivity for a 60 GHz LEPA with $L_1 = 9$ mm, $L_2 = 12$ cm, $G = 2$ cm and $F = 4.8$ cm for (a) boresight and (b) (45, 30) scan.

while the needed directivity is substantial. The LA aperture and G both can be relatively large. Assuming $L_1 = 1.6$ cm (8×8 PA), $L_2 = 20$ cm (100×100 LA), $G = 8$ cm, and $\theta_{o,\max} = 5°$, one can find $\alpha = 6.15$ and $F = 9.55$ cm. Since G is much greater than L_1 (and λ) the smudging effect is minimal and (30) can be solved for the actual desired scan value. Fig. 11 shows the simulated LA aperture illumination and resulting radiation pattern at 75 GHz for this design for boresight and (45°, 45°) beam angles. The boundary of the geometrically found lit region is also shown in each case, demonstrating a remarkable agreement between the geometrical and wave analyses in this case. Simulated directivity is > 37 dB for all values of scan angle within $5°$ of the boresight. Although this represents a significant increase in directivity compared to the standalone PA, the net directivity boost is still 1.8 dB less than the theoretical value of α^2. This loss of directivity can be attributed to the phase errors in the output LA aperture, which become more critical as the size of lit region becomes comparable to the lens aperture.

These examples reveal the key interplay between the depth, scan field of view, and directivity boost of the LEPA system. Low depth configurations ($G/L_1 < 1$) are best suited to applications with wide scan field of view, but offer a modest enhancement in the directivity. The scan field of view cannot be traded for directivity, as smudging effects tend to limit the size of the lit region. Medium depth systems (G comparable to L_1) provide the greatest design flexibility in terms of directivity/scan field of view trade off. When combined with large
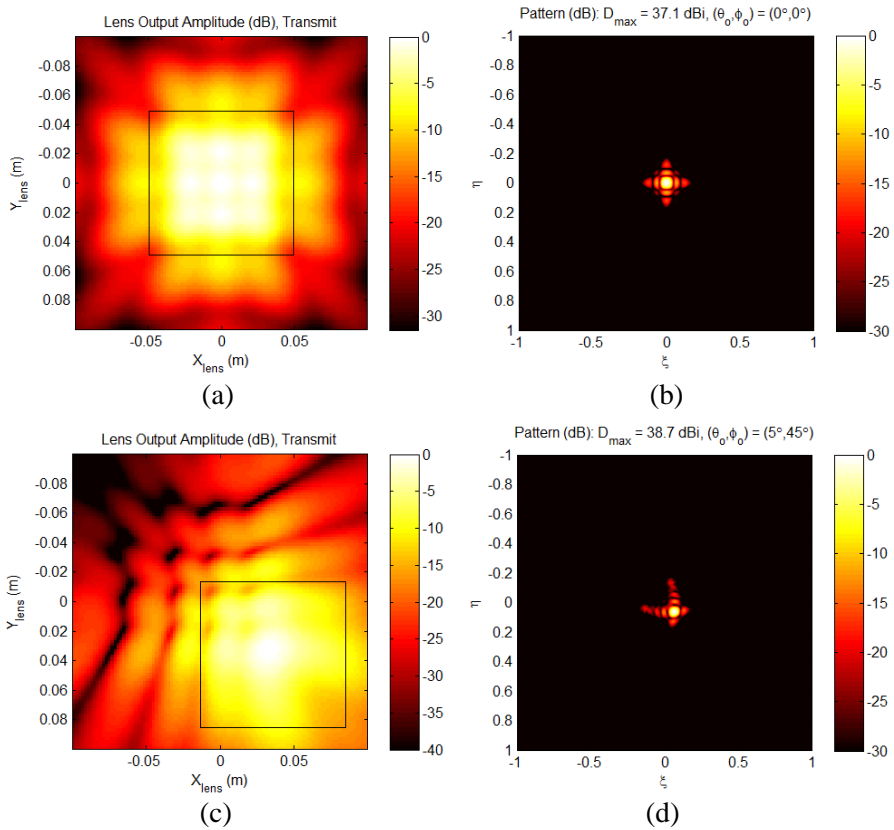
Figure 11. (a) Simulated aperture illumination and (b) radiation pattern for a 75 GHz LEPA with $L_1 = 1.6$ cm, $L_2 = 20$ cm, $G = 8$ cm, and $F = 9.55$ mm for the boresigt beam state. (c) and (d) show the same for $(45°, 45°)$ scan.

LA's they can be designed for wide scan angles and medium directivity boost or for smaller scan and greater directivity enhancement. The directivity boost in medium depth LEPA's is ultimately limited by smudging and is in the range of several dB's. Deep LEPA systems $(G/L_1 \gg 1)$ are best suited for high-gain, narrow-scan applications. Directivity enhancement in these systems can be in tens of dB's for small scan angles $(< 10°)$, but it diminishes quickly for larger scan field of views. Geometrical dimensions of the LEPA system can be chosen based on practical limitations and performance requirement of the specific application.

6. CONCLUSION

The Lens-Enhanced Phased Array (LEPA) configuration was proposed and studied for implementing high-directivity steerable antennas. This topology that combines a small phased array with a much larger fixed lens-array provides a flexible, efficient, compact, and cost-effective method for increasing directivity, without putting penalties on the chip size and DC power consumption. It was shown that adding the lens improves the overall directivity and reduces the scan loss. Also, compared to conventional multi-beam lens systems, the use of the phased array to replace the switchable feed matrix reduces the complexity and overall depth of the antenna system, and allows for some degree of power combining that is particularly desirable at millimeter-wave frequencies. The theory and procedures for designing the lens and finding the phased array coefficients were described at length and their potential application was demonstrated through a number of examples. Although the studies presented here assume an implementation based on a discrete lens-array, the design formulations and results are general and applicable to other planar lens designs, as well as to similar enhanced phased array configurations based on reflectarrays.

ACKNOWLEDGMENT

REFERENCES

1. Koh, K.-J., J. W. May, and G. M. Rebeiz, "A millimeter-wave (40–34 GHz) 16-element phased-array transmitter in 0.18-µm SiGe BiCMOS technology," *IEEE International Solid-State Circuits Conference Digest of Technical Papers (ISSCC)*, Vol. 44, 1498–1509, May 2009.

2. Chan, W. L. and J. R. Long, "A 60-GHz band 2×2 phased-array transmitter in 65-nm CMOS," *IEEE International Solid-State Circuits Conference Digest of Technical Papers (ISSCC)*, Vol. 45, 2682–2695, Dec. 2010.

3. Cohen, E., C. Jakobson, S. Ravid, and D. Ritter, "A thirty two element phased-array transceiver at 60 GHz with RF-IF conversion block in 90 nm flip chip CMOS process," *IEEE Radio Frequency Integrated Circuits Symposium (RFIC)*, 457–460, 2010.

4. Reynolds, S., et al., "A 16-element phased-array receiver IC for 60-GHz communications in SiGe BiCMOS," *IEEE Radio Frequency Integrated Circuits Symposium (RFIC)*, 461–464, 2010.

5. Valdes-Garcia, A., et al., "A SiGe BiCMOS 16-element phased-array transmitter for 60 GHz communications," *IEEE International Solid-State Circuits Conference Digest of Technical Papers (ISSCC)*, 218–219, 2010.

6. Mailloux, R. J., L. Zahn, A. Martinez, and G. Forbes, "Grating lobe control in limited scan arrays," *IEEE Trans. on Antennas and Propagation*, Vol. 27, No. 1, 79–85, Jan. 1979.

7. Fante, R. L., "System study of overlapped subarrayed scanning antennas," *IEEE Trans. on Antennas and Propagation*, Vol. 28, 668–679, Sep. 1980.

8. Abbaspour-Tamijani, A. and K. Sarabandi, "An affordable millimeter-wave beam-steerable antenna using interleaved planar subarrays," *IEEE Trans. on Microwave Antennas and Propagation*, Vol. 51, 2193–2202, Sep. 2003.

9. Abbaspour-Tamijani, A., L. Zhang, and H. K. Pan, "Lens-enhanced phased array antenna system for high directivity beam-steering," *IEEE International Symposium on Antennas and Propagation (APSURSI)*, 3275–3278, 2011.

10. Popovic, D. and Z. Popovic, "Multi-beam antennas with polarization and angle diversity," *IEEE Trans. on Antennas and Propagation*, Vol. 50, 651–657, May 2002.

11. Abbaspour-Tamijani, A., K. Sarabandi, and G. M. Rebeiz, "A millimeter-wave bandpass filter-lens array," *IET Microwaves, Antennas & Propagation*, Vol. 1, 388–395, Apr. 2007.

12. Cheng, C. C. and A. Abbaspour-Tamijani, "Low-loss lens-array for wide-scan millimeter-wave beam-steering," *IEEE Antennas and Propagation Society International Symposium*, 4393–4396, Honolulu, HI, Jun. 2007.

13. Abbaspour-Tamijani, A. and G. M. Rebeiz, "Low-loss bandpass antenna-filter-antenna arrays for applications in quasi-optical systems," *European Microwave Conference*, *Digest of Papers*, 1027–1030, Paris, France, 2005.